SUMOylation promotes de novo targeting of HP1 ± to pericentric heterochromatin

Article *in* Nature Genetics · February 2011

DOI: 10.1038/ng.765 · Source: PubMed

nature genetics

SUMOylation promotes *de novo* targeting of HP1α to pericentric heterochromatin

Christèle Maison[1,2], Delphine Bailly[1,2], Danièle Roche[1,2], Rocio Montes de Oca[1,2], Aline V Probst[1,2,4], Isabelle Vassias[1,2], Florent Dingli[1,3], Bérengère Lombard[1,3], Damarys Loew[1,3], Jean-Pierre Quivy[1,2] & Geneviève Almouzni[1,2]

HP1 enrichment at pericentric heterochromatin is considered important for centromere function. Although HP1 binding to H3K9me3 can explain its accumulation at pericentric heterochromatin, how it is initially targeted there remains unclear. Here, in mouse cells, we reveal the presence of long nuclear noncoding transcripts corresponding to major satellite repeats at the periphery of pericentric heterochromatin. Furthermore, we find that major transcripts in the forward orientation specifically associate with SUMO-modified HP1 proteins. We identified this modification as SUMO-1 and mapped it in the hinge domain of HP1α. Notably, the hinge domain and its SUMOylation proved critical to promote the initial targeting of HP1α to pericentric domains using *de novo* localization assays, whereas they are dispensable for maintenance of HP1 domains. We propose that SUMO-HP1, through a specific association with major forward transcript, is guided at the pericentric heterochromatin domain to seed further HP1 localization.

Heterochromatin at pericentric domains represents a paradigm for understanding how a functional nuclear domain is established and maintained. Studies in *Schizosaccharomyces pombe* and *Drosophila* have advanced our knowledge concerning basic mechanisms and conserved components in the organization of the domain[1]. In particular, HP1 proteins that accumulate in these domains are highly conserved from *S. pombe* to mammals. However, in mammalian cells, how HP1 is specifically targeted *de novo* to initiate formation of a domain of accumulation as found in pericentric heterochromatin[2,3] remains mysterious. The recognition of H3K9me3 by HP1 (refs. 4,5), which exemplifies the paradigm of the reader model in the histone code hypothesis[6,7], does not necessarily provide on its own a *de novo* specific targeting mechanism. One should also consider other HP1 binding partners[8,9], potential post-translational modifications[10] and the elusive RNA that has been linked to the presence of HP1 at pericentric heterochromatin[11,12]. Although transcripts from major satellite DNA repeats have been identified[13,14], a functional connection between specific RNAs and HP1 has not yet been established. Taken together, these data prompted us to explore further the HP1-RNA connection and particular post-translational modifications or partners that could provide a means for the *de novo* targeting of HP1 to pericentric heterochromatin, thereby helping to define this specific subnuclear compartment.

RESULTS

SUMO-1–HP1α interacts with forward major RNA

We first verified that repetitive DNA sequences in mouse centromeres, known as major and minor satellites in pericentric and centric heterochromatin, respectively[15], can be transcribed in both orientations. All the transcripts detected by RT-PCR analysis with strand-specific primers for major or minor satellites had various sizes corresponding to multiple repeats of their basic units (**Fig. 1a**). We next examined whether some of these transcripts could be stably found in the nucleus. As a reference for comparison, we used the well-defined organization of chromocenters with major satellite repeats surrounded by minor satellite DNA (**Fig. 1b**, left, DNA fluorescence *in situ* hybridization (FISH))[2]. For this, we exploited fluorescently labeled locked nucleic acid (LNA) probes for RNA FISH that specifically detect major and minor transcripts in either forward or reverse orientation. Whereas minor RNAs were barely detectable, LNA probes for major RNAs in both orientations revealed a substantial number of nuclear spots frequently associated with or close to chromocenters (**Fig. 1b**, middle). These signals were not a result of DNA cross-hybridization, as they were undetectable after RNase treatment (**Supplementary Fig. 1**). With some variations from cell to cell suggesting cell cycle modulation, reverse major RNAs were usually detected as fewer and larger spots (**Fig. 1b**, middle, red), and forward major RNA signals were smaller in size and present in higher numbers (**Fig. 1b**, green). Notably, these forward major RNAs were consistently at the periphery of HP1α domains (**Fig. 1b**, right, immuno-RNA FISH and **Supplementary Fig. 2a**). Because active transcription occurs frequently in the external part of chromosomal domains by DNA looping out[16], they may represent primary transcripts stably maintained at the site of transcription. Notably, HP1α accumulated at major satellite domains, away from minor satellites, which were juxtaposed (**Fig. 1c** and

[1]Institut Curie, Centre de recherche, Paris, France. [2]Centre National de la Recherche Scientifique (CNRS), Unité Mixte de Recherche UMR218, Laboratory of Nuclear Dynamics and Genome Plasticity, Paris, France. [3]Laboratory of Proteomic Mass Spectrometry, Paris, France. [4]Present address: CNRS, UMR 6247 GreD, Clermont Université, INSERM U931, Aubière, France. Correspondence should be addressed to J.-P.Q. (jpquivy@curie.fr) or G.A. (genevieve.almouzni@curie.fr).

Received 4 August 2010; accepted 18 January 2011; published online 13 February 2011; doi:10.1038/ng.765

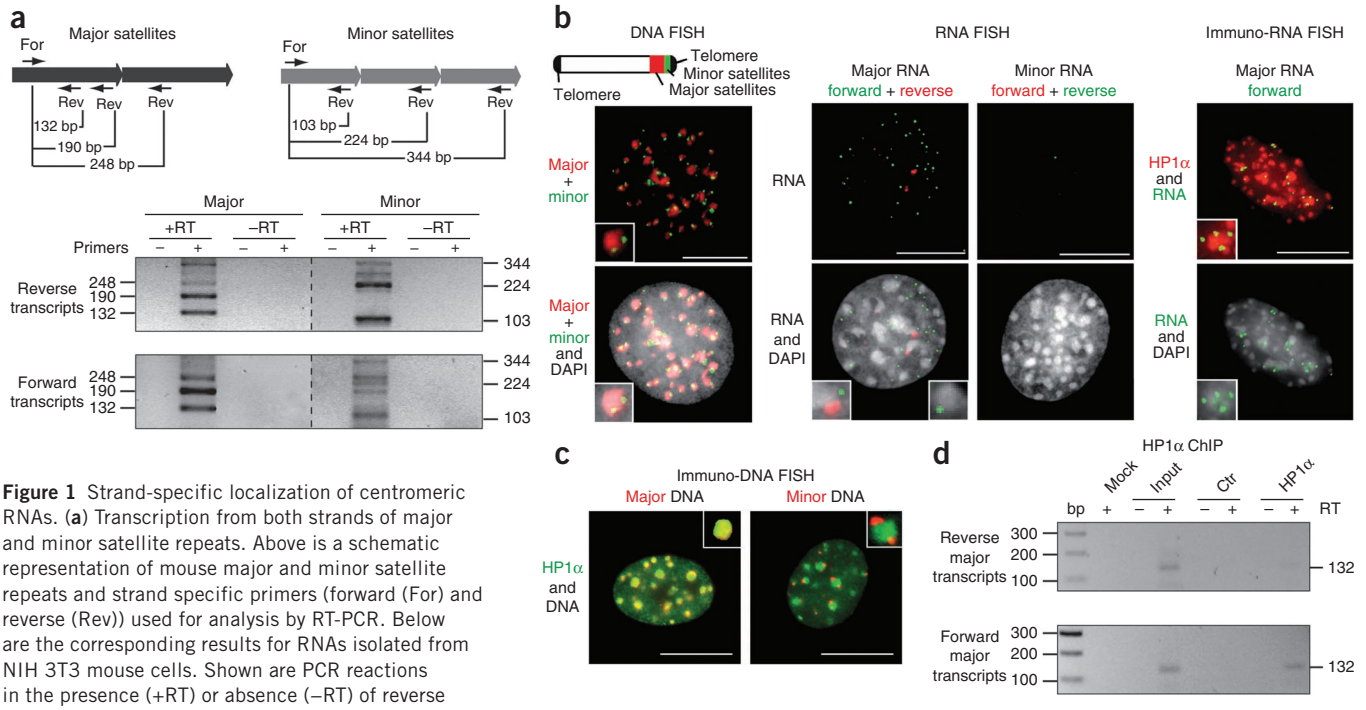

Figure 1 Strand-specific localization of centromeric RNAs. (**a**) Transcription from both strands of major and minor satellite repeats. Above is a schematic representation of mouse major and minor satellite repeats and strand specific primers (forward (For) and reverse (Rev)) used for analysis by RT-PCR. Below are the corresponding results for RNAs isolated from NIH 3T3 mouse cells. Shown are PCR reactions in the presence (+RT) or absence (–RT) of reverse transcriptase or primers as controls. (**b**) Nuclear localization of centromeric RNA compared to major and minor satellite DNA in NIH 3T3 cells. At left is DNA FISH. Scheme of an acrocentric mouse chromosome with telomeres (black), major (red) and minor (green) satellites. Major (red) and minor (green) satellites are shown, along with a merged image of major and minor satellites and DAPI-stained DNA. In the middle is RNA FISH. We localized major (forward in green and reverse in red) and minor (forward in red and reverse in green) RNAs with strand-specific LNA probes and show a merged image of DAPI and centromeric RNA staining. Insets show magnifications of chromocenters. At right is immuno-RNA FISH. Forward major RNAs (green) and HP1α antibody (red) staining are shown, along with a merged image of DAPI and major RNA staining. Scale bar, 10 μm. (**c**) HP1α accumulation at major satellite DNA domains. Immuno-DNA FISH with anti-HP1α antibodies (green) and major or minor satellite DNA (red) probes. Insets are as in **b**. Scale bar, 10 μm. (**d**) RNAs associated with HP1α. Chromatin immunoprecipation (ChIP) experiments using pre-immune serum (Ctr) or anti-HP1α antibodies (HP1α) analyzed by strand-specific RT-PCR as indicated. We show PCR reactions with (+RT) or without (–RT) reverse transcriptase and without cDNA (mock) as controls. The input corresponds to the soluble chromatin before ChIP.

Supplementary Fig. 2b, immuno-DNA FISH)[2]. We then examined further the possible *in vivo* association of major RNAs with major satellite domains by other methods. Under conditions that preserved the RNAs, we immunoprecipitated heterochromatin-associated material with a specific HP1α antibody. We found a clearly higher amount of forward major transcripts compared to reverse transcripts (**Fig. 1d**). Taken together, our data highlight a particular link between major RNA in the forward orientation and pericentric heterochromatin.

Whereas HP1α can bind RNA *in vitro*[12], specific binding to a given transcript has been reported so far only for telomeric repeat-containing RNA (TERRA)[17]. Using GST-tagged HP1α full-length protein or fragments thereof and radioactively labeled centromeric RNA probes (**Fig. 2a**), we found that the hinge domain (H) of HP1α strongly recognized both forward and reverse centromeric RNA probes, whereas the chromo-hinge (CD+H) and the hinge-chromoshadow (H+CSD) domains showed a lower binding capacity. Under these conditions, we did not detect binding between full-length HP1α and RNAs (**Fig. 2a**). These results suggest that the central hinge domain may adopt a different conformation in the full-length protein, possibly constrained by the chromo and/or chromoshadow domain. This raised the possibility that HP1α could actually bind RNA *in vivo* and that this interaction can be regulated. To investigate this hypothesis, we aimed to identify proteins from nuclear cell extracts that associated with centromeric RNAs using *in vitro* transcribed biotin-labeled forward major or minor RNAs immobilized on streptavidin beads (**Fig. 2b** and **Supplementary Fig. 3a**). Mass spectrometry analysis of the RNA-associated proteins identified mainly heterogeneous nuclear ribonucleoproteins (hnRNPs) and proteins involved in RNA processing (**Supplementary Fig. 3b** and **Supplementary Table 1**) including vigilin, RNA helicase A (RHA) and Ras-GAP SH3 domain–binding protein (G3bp), which were all validated by protein blotting (**Fig. 2c**). Vigilin and the *Drosophila* RHA ortholog, maleless (MLE), are thought to play roles in heterochromatin formation and X-chromosome dosage compensation, respectively[18,19], whereas G3bp may be involved in RNA metabolism[20]. Notably, under these experimental conditions, we did not detect any significant association between HP1α and major or minor RNAs either by mass spectrometry (**Supplementary Fig. 3b**) or protein blotting (**Fig. 2c**). Given our *in vitro* observations (**Fig. 2a**), we wondered whether post-translational modification of HP1α could promote *in vivo* HP1α binding to RNA. Indeed, HP1 can be phosphorylated[10], and in fission yeast, Swi6 (HP1) is SUMOylated *in vivo*[21]. Furthermore, defective SUMOylation of Swi6 results in a substantial reduction in heterochromatin stability. This prompted us to repeat our RNA pull-down strategy with nuclear extracts prepared in the presence of a cocktail of phosphatase inhibitors and N-ethylmaleimide (NEM), a strong inhibitor of SUMO isopeptidases[22]. Remarkably, protein blotting with an HP1α antibody revealed a slower migrating band in the input for HP1α that was not detected in the absence of NEM and that was then specifically enriched in precipitates with forward major RNAs corresponding to either one or two satellite repeats length

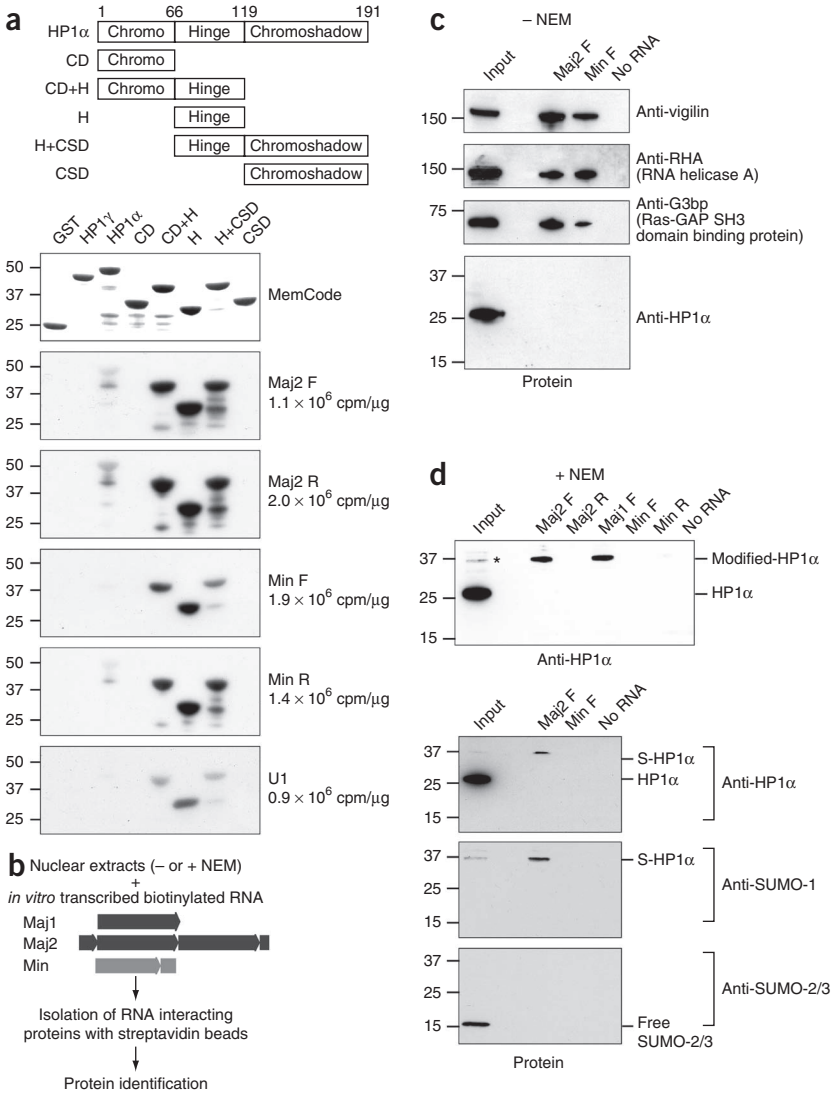

Figure 2 SUMO-1–modified HP1α interacts specifically with forward major RNAs. (**a**) Northwestern blot using recombinant GST-HP1γ, GST-HP1α or GST-HP1α domain fragments and *in vitro* transcribed radioactively labeled RNAs; forward (F) and reverse (R) major (Maj2) and minor (Min) RNAs and U1 was used as the negative control. (**b**) Experimental scheme. (**c**) RNA pull down using forward major (Maj2 F) or minor (Min F) RNAs or no RNA as the negative control, in the absence of NEM. We show protein blot analysis with vigilin, RHA, G3bp or HP1α antibodies. Input is 10% of nuclear extracts. (**d**) RNA pull down using forward (F) and reverse (R) major (Maj2 F, Maj1 F, Maj2 R) or minor (Min F, Min R) RNAs as baits or no RNA as the control in the presence of NEM. Protein blot analysis using HP1α, SUMO-1 and SUMO-2/3 antibodies revealed endogenous unmodified HP1α (HP1α), modified HP1α, SUMO-HP1α (S-HP1α) and free SUMO-2/3. Input is 10% of nuclear extracts. *SUMO-HP1α in the input.

(**Fig. 2d**; Maj1 F or Maj2 F). This band, with an approximate additional molecular mass of ~11 kDa compared to HP1α, might represent a ubiquitin or a SUMO moiety. We confirmed that this slower-migrating form was modified by SUMO-1 but not SUMO-2/3, using specific antibodies (**Fig. 2d**). We obtained similar results with antibodies specific to HP1β and HP1γ (**Supplementary Fig. 3c**), indicating that all HP1 isoforms can potentially be SUMOylated *in vivo* and are specifically retrieved with forward major RNAs. Although the forward major RNA pulls down SUMO-1–HP1α, we estimated that only a small percentage of HP1α was SUMO-1 modified *in vivo* (less than 1% of the total protein from nuclear extracts; **Fig. 2d**). This low representation is in agreement with rapid cycles of SUMOylation and deSUMOylation, as reported for other proteins weakly detected in a SUMO-modified state *in vivo*[23,24].

The hinge domain of HP1α is a major target for SUMOylation

To confirm independently that HP1α is SUMOylated *in vivo*, we co-transfected HA-tagged HP1α (e-HP1α) and GFP-SUMO-1 into NIH 3T3 cells to prepare total cell extracts and carried out immunoprecipitations with anti-HA beads under conditions that preserved the SUMO modification[25]. Protein blot analysis using GFP antibodies clearly revealed a band corresponding to GFP-SUMO-e-HP1α (**Supplementary Fig. 4a**), demonstrating unambiguously that HP1α can be SUMOylated *in vivo*. To determine which region of HP1α was modified by SUMO, we next used an *in vitro* SUMOylation assay with either wild-type (W) or mutant (M) SUMO-1 protein in the presence of E1-activating and E2-conjugating (Ubc9) SUMO enzymes and various GST-HP1α domains (**Fig. 3a**). Protein blot analysis using GST antibodies showed SUMO modification on the full-length HP1α, the chromo-hinge, the hinge-chromoshadow and the hinge domains, with the latter domain showing the highest level of SUMOylation (**Fig. 3b** and **Supplementary Fig. 4b**, asterisks). This is also true when using SUMO-2 or SUMO-3 (**Supplementary Fig. 4c**). These results revealed that the hinge, the same domain of HP1α that displayed RNA-binding activity (**Fig. 2a**), is a target for SUMOylation. Because the fusion of Ubc9 to a substrate provides a convenient way to increase its SUMOylation[26], we also verified with a GST-HP1α-Ubc9 fusion protein that we could enhance SUMO-1 modification of HP1α *in vitro* without adding the E2 enzyme (**Fig. 3c**). Then, using the GST-HP1α hinge and SUMO-1 proteins as above (**Supplementary Fig. 5a**), we further identified specific SUMOylated residues on HP1α by mass spectrometry. In the hinge domain, among the 13 lysines that are potential targets for SUMOylation, we found that Lys84 of HP1α in the peptide EKSEGNK (with the underlined K indicating Lys84) was unequivocally identified as SUMOylated by mass (with high accuracy in the Orbitrap; **Fig. 3d**, right spectra, arrow) and sequence (by tandem mass spectrometry (MS/MS) in the QSTAR mass spectrometer; **Fig. 3d**; the y and b ions are shown). However, we also found other potentially SUMOylated lysines in HP1α (for example, KMoxK, SKK, KYK or YKK; **Supplementary Fig. 5b**,**c**), indicating alternative usage of various lysine residues. We thus mutated successively each of the individual 13 lysines to arginines and performed *in vitro* SUMOylation assays as above and *in vivo* co-transfections as in **Supplementary Figure 4a**. We observed in all cases that once we mutated one residue, an alternative SUMOylation site was used

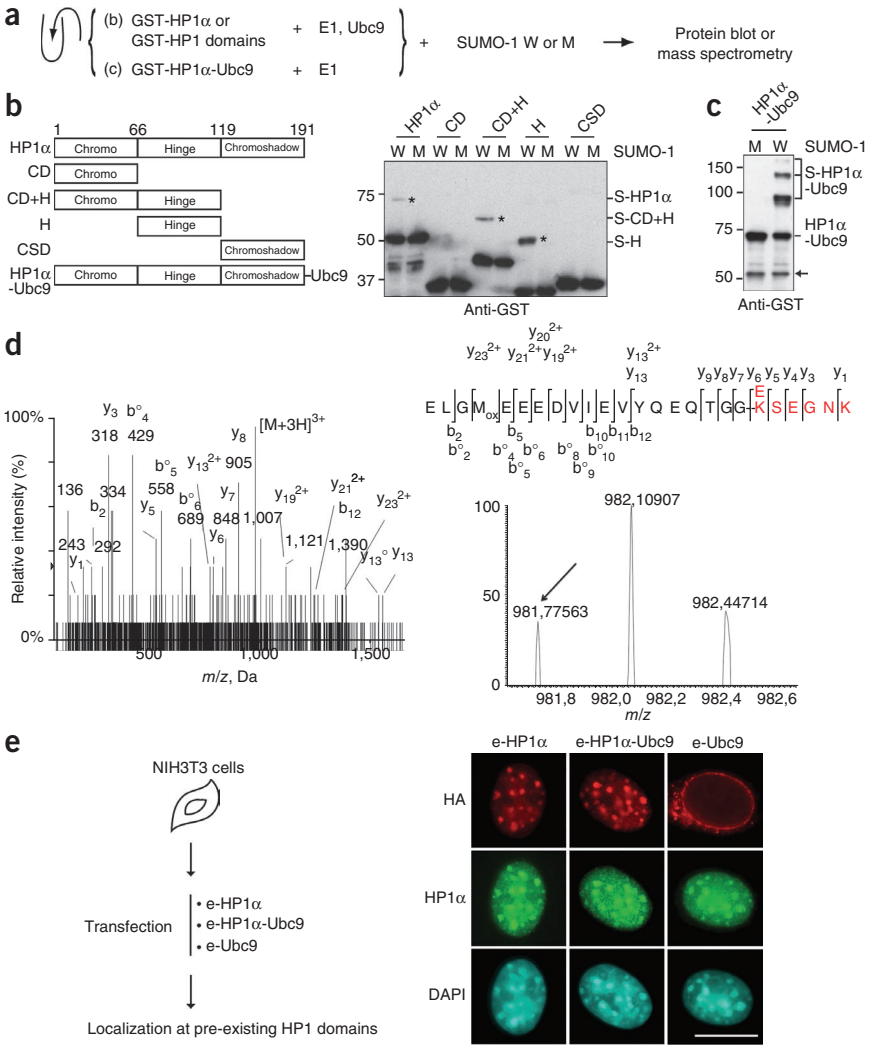

Figure 3 SUMOylation of HP1α occurs at its hinge domain *in vitro*. (**a**) Experimental scheme. (**b**) HP1α SUMOylation *in vitro*. At left is the schematic representation of full-length HP1α and fragments thereof. At right, the protein blot analysis of the SUMOylation reaction mixture with GST antibodies revealed the positions of SUMO-1–modified full-length HP1α (S-HP1α) or fragment domains (S-CD+H and S-H) marked by an asterisk. W, wild type; M, mutant. (**c**) HP1α-Ubc9 SUMOylation *in vitro*. Protein blot analysis of the SUMOylation reaction mixture with GST antibodies revealed the positions of SUMO-1–modified HP1α-Ubc9 (S-HP1α-Ubc9) and unmodified HP1α-Ubc9. The arrow indicates a degradation product of GST-HP1α-Ubc9. (**d**) Mass spectrometry analysis of the *in vitro* SUMO-1–modified HP1α hinge fragment. Shown are the mass spectrometry (right) and tandem mass spectrometry (left) fragmentation spectra of the tryptic peptide corresponding to residues 79–97 of SUMO-1 (top right, black) and residues 83–89 of HP1α (EKSEGNK; red) where Lys84 is sumoylated. The precursor ion mass was fragmented and acquired in QStar (m/z 981.8 (3+); left) and Orbitrap (m/z 981.77563, mass deviation 2 ppm; right, arrow) mass spectrometers. The majority of the fragment ions could be assigned to the y or b ion series, as annotated in the spectra and peptide sequence (top right). (**e**) Localization of e-HP1α and e-HP1α-Ubc9 in Triton-extracted NIH 3T3 cells. At left is the experimental scheme. At right is immunofluorescence using HA (red) and HP1α (green) antibodies. Scale bar, 10 μm.

(data not shown), showing the usage of more than one SUMOylation site and corroborating our mass spectrometry data. This suggests a lack of a strict requirement for a 'specific' SUMO-modified residue.

SUMOylation of HP1α promotes its targeting

Because the fusion of Ubc9 to HP1α increases SUMOylation efficiency *in vitro* (**Fig. 3c**), we thus generated an HP1α-Ubc9-HA fusion construct (e-HP1α-Ubc9) for *in vivo* expression and further analysis in a cellular context. Transfection of e-HP1α-Ubc9 or e-HP1α into NIH 3T3 cells lead to comparable levels of proteins being expressed (**Supplementary Fig. 6a**,**b**; anti-HA). Notably, we detected a higher amount of SUMO-modified e-HP1α-Ubc9. In total cell extracts, we found that e-HP1α-Ubc9 was mainly SUMO-2/3 modified, reflecting the readily available endogenous SUMO-2 and SUMO-3 proteins compared to the limited amount of free endogenous SUMO-1 protein in cells (compare SUMO-1 with SUMO-2/3 inputs in **Fig. 2d**)[23]. This could be compensated for by providing exogenous SUMO-1 by transient transfection (**Supplementary Fig. 6c**). These *in vivo* results underline the fact that HP1α can be modified by SUMO-1, SUMO-2 or SUMO-3 depending on the available substrate, as shown *in vitro* (**Fig. 3b,c** and **Supplementary Fig. 4b**,**c**). We verified that the catalytic activity of the fused Ubc9 was directly involved in HP1α SUMOylation enhancement using a Ubc9 catalytic mutant fused to HP1α (e-HP1α-Ubc9C93S). In comparaison with wild-type (wt) e-HP1α-Ubc9, we detected a strongly reduced SUMOylation of e-HP1α-Ubc9C93S (**Supplementary Fig. 6c**).

Next, we examined e-HP1α-Ubc9 and e-HP1α localization in NIH 3T3 cells. Both of them could accumulate at pericentric domains where endogenous HP1α is already located (**Fig. 3e**). Thus, under these conditions, promoting HP1 SUMOylation did not give a particular advantage for the recruitment and maintenance of exogenous HP1 to pre-existing HP1 domains of accumulation. Next, we wondered whether HP1α SUMOylation could be required more specifically for a *de novo* targeting of HP1α to heterochromatin domains. To test this hypothesis, we used mouse embryonic fibroblasts (MEFs) derived from *Suv39h* double-null mice in which the H3K9me3 mark and HP1α were no longer enriched at pericentric heterochromatin[11,27] (**Fig. 4**). Transfection with exogenous Myc-SUV39H1 could restore the proper localization of these marks (**Fig. 4b**)[5,28]. As we postulated that the interaction between major RNAs and SUMOylated HP1α targets HP1α to pericentric domains, we first verified that we could detect major RNAs by RNA-FISH in *Suv39h* double-null MEFs (**Supplementary Fig. 7a**). We then transiently transfected *Suv39h* double-null cells with e-HP1α or e-HP1α-Ubc9 in the absence of Myc-SUV39H1 and verified that the proteins were expressed at comparable levels (**Fig. 4c**). We could not detect the typical localization to chromocenters in cells transfected with e-HP1α (**Fig. 4c**). In contrast, in about 10% of cells transfected with e-HP1α-Ubc9, we found a faint but detectable pericentric localization 6 h post transfection. Remarkably, in the latter case,

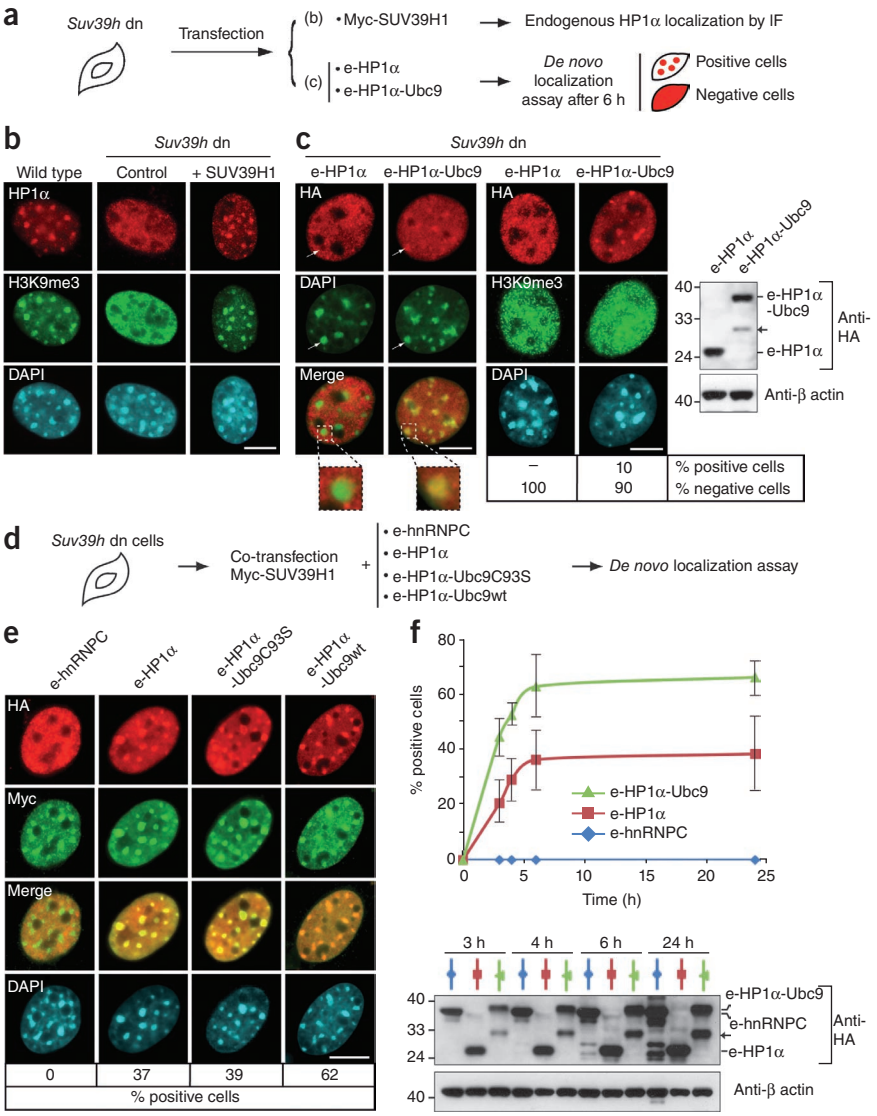

Figure 4 SUMOylation of HP1α promotes its targeting and accumulation at pericentric heterochromatin. (**a**) Experimental scheme. (**b**) Endogenous HP1α (red) and H3K9me3 (green) localization in wild-type and in *Suv39h* double-null (dn) cells by immunofluorescence (IF). Transfection of Myc-SUV39H1 in *Suv39h* double-null cells restored HP1α and H3K9me3 localization in DAPI-dense domains. Scale bar, 10 μm. (**c**) *De novo* localization of e-HP1α or e-HP1α-Ubc9 in *Suv39h* double-null cells by immunofluorescence. At left, HA (red) and DAPI (green) staining with ×3 magnification of selected chromocenters (arrows). In the middle, HA (red) and H3K9me3 (green) staining. For each condition, we examined 300 transfected cells and calculated the percentage of cells with HA signal enriched (positive) or not (negative) at pericentric domains. Scale bar, 10 μm. At right, comparison of protein expression by protein blot, revealing HA and β actin. The arrow indicates degradation of e-HP1α-Ubc9. (**d**) Experimental scheme. (**e**) *De novo* localization of e-hnRNPC, e-HP1α, e-HP1α-Ubc9C93S and e-HP1α-Ubc9wt in *Suv39h* double-null cells co-transfected with Myc-SUV39H1 by immunofluorescence to reveal HA (red) and Myc (green). The percentage of positive cells was calculated as in **c**. Scale bar, 10 μm. (**f**) Time-course analysis of the *de novo* localization of e-hnRNPC, e-HP1α and e-HP1α-Ubc9 in *Suv39h* double-null cells co-transfected with Myc-SUV39H1. At the top, the percentage of positive cells as a function of the time after transfection is represented. Symbols indicate the mean, and error bars indicate the s.d. of three independent experiments (300 co-transfected cells counted in each condition). At the bottom is a comparison of protein expression as in **c**. The arrow indicates degradation of e-HP1α-Ubc9.

we could not detect H3K9me3 accumulation at pericentric heterochromatin (**Fig. 4c** and **Supplementary Fig. 7b**), whereas H3K9me1 was clearly visible at these domains in all *Suv39h* double-null cells (**Supplementary Fig. 7c**). Thus, a targeting of e-HP1α-Ubc9 to pericentric heterochromatin could occur in the absence of SUV39H1-dependent H3K9me3. However, whereas e-HP1α-Ubc9 was more efficiently targeted than e-HP1α, the low fraction of cells showing this staining suggested that following this initial recruitment, retention at pericentric domains was rather inefficient. We thus modified our assay to monitor the localization of e-HP1α or e-HP1α-Ubc9 to pericentric chromatin in the presence of Myc-SUV39H1 assuming that H3K9me3 could promote stabilization (**Fig. 4d**). Immunofluorescence analysis revealed that e-HP1α, e-HP1α-Ubc9C93S and e-HP1α-Ubc9wt accumulated at pericentric heterochromatin when co-transfected with Myc-SUV39H1, in contrast to a negative control protein, e-hnRNPC (**Fig. 4e**). Notably, e-HP1α-Ubc9wt localized to these domains more efficiently than e-HP1α and e-HP1α-Ubc9C93S (62% versus 37% and 39% of positive cells, respectively, 6 h post transfection) for comparable levels of expressed proteins (**Supplementary Fig. 8a**). Also, the e-HP1α and e-HP1α-Ubc9C93S overall staining in the nucleus was rather diffuse compared to e-HP1α-Ubc9wt staining, suggesting that a significant fraction of e-HP1α and e-HP1α-Ubc9C93S is not localized at pericentric heterochromatin (see **Fig. 4e** and **Supplementary Fig. 8b** and its legend for details). Taken together, these results indicate that enhancing SUMOylation on HP1α promotes a more efficient accumulation at pericentric heterochromatin. We then performed a time-course analysis to compare the appearance of HP1α at pericentric heterochromatin in *Suv39h* double-null cells co-transfected with Myc-SUV39H1 and e-HP1α or e-HP1α-Ubc9 (**Fig. 4f**). We found that e-HP1α-Ubc9 always localized more efficiently to pericentric heterochromatin compared to e-HP1α (52% versus 31% of positive cells, respectively, 4 h post transfection) for comparable levels of expressed proteins along the time-course analysis (**Fig. 4f**). The different efficiencies with which these proteins localized to pericentric heterochromatin support the hypothesis of SUMOylation acting as a limiting step to promote HP1α targeting. In support of this hypothesis, although toxic, the direct fusion of SUMO-1 to HP1α showed an even more efficient accumulation compared to e-HP1α-Ubc9 (see **Supplementary Fig. 9** and its legend for details). The simplest interpretation for this is that a higher amount of SUMOylated protein provided by HP1α-Ubc9 fusion would allow a rapid targeting to pericentric domains, whereas HP1α alone would be delayed by the time needed to undergo an entire cycle of SUMOylation. Overall, our data underline the importance of the HP1α SUMO modification before HP1α targeting to pericentric heterochromatin.

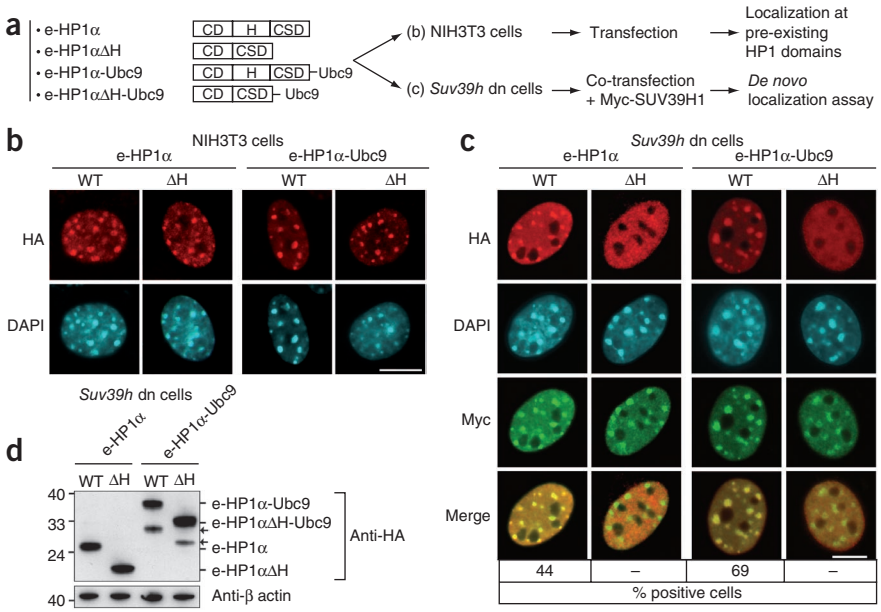

Figure 5 The hinge domain is required for *de novo* localization of HP1α at pericentric heterochromatin. (**a**) Experimental scheme. (**b**) Localization of wild-type (WT) or mutant (ΔH) e-HP1α and e-HP1α-Ubc9 in NIH 3T3 cells by immunofluorescence using HA antibodies (red) 24 h after transfection. Scale bar, 10 μm. (**c**) *De novo* localization of wild-type (WT) or mutant (ΔH) e-HP1α and e-HP1α-Ubc9 in *Suv39h* double-null cells co-transfected with Myc-SUV39H1 by immunofluorescence using HA (red) and Myc (green) antibodies 6 h after transfection. For each condition, we calculated the percentage of cells with the HA signal enriched at the pericentric domains (positive cells). Scale bar, 10 μm. (**d**) Comparison of protein expression corresponding to the experiment in **c** by protein blot using HA and β actin antibodies. Arrows indicate degradation products of e-HP1α-Ubc9 and e-HP1αΔH-Ubc9.

The hinge domain is required for *de novo* localization of HP1α

Given that the hinge domain, which shows RNA-binding properties[12], is the target for SUMOylation at multiple sites (**Fig. 3b**), we generated mutants of e-HP1α and e-HP1α-Ubc9 lacking the hinge domain and assayed whether they could specifically localize *de novo* to pericentric heterochromatin in *Suv39h* double-null cells. After transfection of e-HP1αΔH and e-HP1αΔH-Ubc9 constructs in NIH 3T3 cells, we found that the hinge domain was perfectly dispensable to localize HP1α at pre-existing HP1 domains in a 'maintenance assay' (**Fig. 5a**,**b**) as reported in *Drosophila* Kc167 cells[29]. Notably, when using *Suv39h* double-null cells for our *de novo* localization assay, after co-transfection with Myc-SUV39H1, the e-HP1α mutant lacking the hinge domain did not localize at pericentric heterochromatin, in contrast to the wild-type protein, which did accumulate at these domains (44% positive cells; **Fig. 5c**). We verified that all transfected proteins were expressed at comparable levels (**Fig. 5d**). Even when Ubc9 was fused to the mutant protein, we did not detect localization of e-HP1αΔH-Ubc9 at pericentric domains. These data clearly show that the hinge domain, the SUMO modification and the association with major RNAs are critical for *de novo* localization of HP1α at pericentric heterochromatin.

DISCUSSION

Based on our data, we propose a model for the *de novo* targeting and local accumulation of HP1α at pericentric heterochromatin by a multistep mechanism involving initial SUMO-dependent targeting as a 'seeding' step (**Fig. 6**, '1'). This SUMO modification imposed in the hinge domain of HP1 would leave the chromo and chromoshadow domains available for other interactions with heterochromatin proteins (as represented in **Fig. 6**). Subsequent 'chromatin marking' steps would follow, including SUV39-dependent H3K9me3 to ensure HP1 stabilization (**Fig. 6**, '2') and accumulation through a self-enforcing loop (**Fig. 6**, '3')[1]. Our identification of a specific association between SUMO1-HP1α and major RNAs in the forward orientation (**Fig. 2**) provides a molecular basis for the 'seeding' step. Such association may help guide SUMO-HP1α specifically to pericentric heterochromatin. The specificity of the interaction promoted by SUMOylation, either by the sequence, by particular structures formed by these RNAs or by known HP1 partners[9], remains to be determined. Importantly, the HP1-RNA interaction is specific for the forward strand, which is purine rich and may thus adopt a distinct structure. Furthermore, it will be interesting to examine potential SUMO-binding protein candidates[30]. Following the 'seeding' event, coordination with SUV39-mediated H3K9 methylation would be key for HP1α stabilization. Although this step could formally be independent of SUMOylation, it is possible that SUMO-HP1 and RNA interaction may promote additional interactions with other partners (such as SUV39) and enhance SUV39 enzymatic activity. In this way, the seeding event might favor

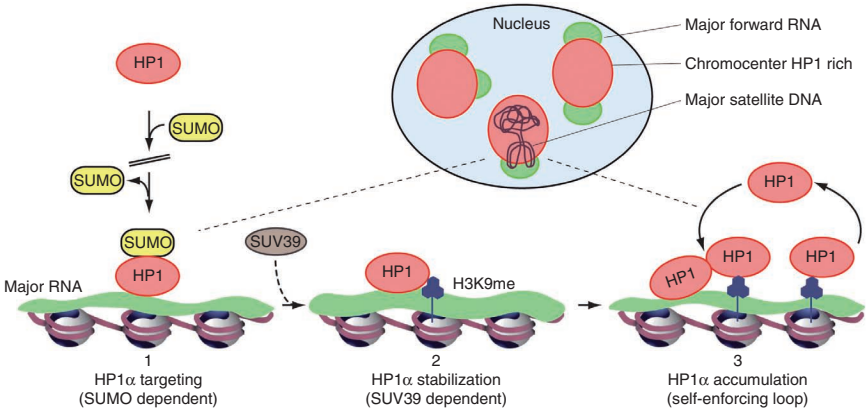

Figure 6 Model for a *de novo* HP1α targeting to pericentric heterochromatin. A schematic representation of a nucleus with pericentric domains enriched in HP1 (red) is depicted showing the nuclear noncoding forward major RNA (green) at the periphery. HP1 (red), most likely as part of a complex, becomes SUMOylated. This SUMO-modified form of HP1α recognizes and binds to major RNAs (green) at pericentric heterochromatin, providing specificity to the initial targeting of HP1α to these domains (1). HP1α stabilization is then ensured by the recognition of H3K9me3 (blue) introduced by SUV39 (light brown) (2). Further HP1α accumulation involves a 'self-enforcing' loop in which new HP1α directly binds to chromatin by multimerizing with other HP1α molecules or by associating with other proteins and/or newly methylated H3K9 (3).

further stabilization steps to establish a robust system for the maintenance of heterochromatin domains. Given that several proteins involved in heterochromatin stability have been shown to bind SUMO conjugates[31], it is tempting to speculate that they could also bind SUMO-HP1. Future work should address how and where HP1 gets SUMOylated and which enzymes trigger both its SUMOylation and deSUMOylation as well as the impact on centromere function. Given the conserved importance of HP1 from fission yeast to mammals[3,32], further investigation of these issues in various organisms should help to define some general principles.

We detected forward RNAs as long species (several repeat lengths) (**Fig. 1a**) and showed that they localize at the periphery of pericentric domains (**Fig. 1b** and **Supplementary Fig. 2a**); however, we did not detect small double-stranded RNA corresponding to major satellites as described for the maintenance of heterochromatin in *S. pombe*[1,33]. It is notable that even in *S. pombe*, primal RNAs have been reported to be important for heterochromatin formation[34]. Although we do not exclude an RNAi pathway in connection with heterochromatin in mammalian cells[35,36], the fact that we detected long noncoding RNAs that are stably located in the nucleus just at the periphery of major satellite domains is very compelling. This is reminiscent of other long nuclear noncoding RNA, such as the lncRNA HOTAIR, proposed to serve as a modular scaffold for histone modification complexes involved in Polycomb function[37], or Xist, which is critical to establish the silent state of the inactive X in mammals. Moreover, Xist RNA is known to be critical in setting up a *de novo* silent domain at specific times during development[38,39]. In this respect, the situation of early development in mice[40,41] is particularly interesting because a burst of transcription of major RNAs occurs just before the formation of HP1 domains of accumulation on the paternal genome[42]. Thus, it is tempting to speculate that SUMOylation could be critical also at this time and perhaps during other developmental time windows. This mechanism could apply to certain cell types when major rearrangements of the genome occur as observed during spermatogenesis[43], differentiation[44,45], reprogramming in the mouse germ line[46], in specialized cell types like Rod photoreceptor cells[47] or even in the formation of senescence-associated heterochromatin foci (SAHF)[48].

Beyond HP1, the concept that a modification, like SUMO, imposed on a chromatin protein could promote localization guided by a particular transcript in the nucleus should be explored. One may wonder whether similar mechanisms also apply to the formation of other local domains of accumulation or nuclear compartments such as Polycomb or insulator bodies.

METHODS

Methods and any associated references are available in the online version of the paper at http://www.nature.com/naturegenetics/.

Note: Supplementary information is available on the Nature Genetics website.

ACKNOWLEDGMENTS

We thank A. Bird, D. Shapiro, R. Hay, T. Jenuwein, R. Losson and J. Seeler for constructs and reagents. We thank W. Faigle for mass spectrometry support, G. Cappello for helpful discussions, A. Cook for critical reading and P. Le Baccon at the Curie Imaging Platform. G.A.'s laboratory is funded by la Ligue Nationale contre le Cancer (Equipe labellisée la Ligue), Curie Programme Incitatif et Collaboratif (PIC) Programs, the European Network of Excellence Epigenome (LSHG-CT-2004-503433), ACI-2007-Cancéropôle IdF 'Breast cancer and Epigenetics', Agence Nationale de la Recherche (ANR) 'EcenS' ANR-09-BLAN-0257-01, INCa 'GepiG', European Research Council (ERC) Advanced Grant 2009-AdG-20090506, and D.L.'s laboratory was funded by le Cancéropôle Ile-de-France and l'INCA.

AUTHOR CONTRIBUTIONS

C.M., J.-P.Q. and G.A. conceived and designed the experiments. C.M., D.B. and J.-P.Q. performed most of the experiments. D.R. and I.V. performed immuno-DNA FISH and immuno-RNA FISH. A.V.P. performed RNA FISH. F.D., B.L. and D.L. performed and analyzed mass spectrometry data using samples prepared by R.M.d.O. and they wrote together the corresponding parts. C.M. generated all figures. C.M., J.-P.Q. and G.A. analyzed the data. C.M. and G.A. wrote the paper. All authors contributed to final editing of the manuscript.

COMPETING FINANCIAL INTERESTS

The authors declare no competing financial interests.

Published online at http://www.nature.com/naturegenetics/.
Reprints and permissions information is available online at http://npg.nature.com/reprintsandpermissions/.

1. Grewal, S.I. & Jia, S. Heterochromatin revisited. *Nat. Rev. Genet.* **8**, 35–46 (2007).
2. Guenatri, M., Bailly, D., Maison, C. & Almouzni, G. Mouse centric and pericentric satellite repeats form distinct functional heterochromatin. *J. Cell Biol.* **166**, 493–505 (2004).
3. Probst, A.V., Dunleavy, E. & Almouzni, G. Epigenetic inheritance during the cell cycle. *Nat. Rev. Mol. Cell Biol.* **10**, 192–206 (2009).
4. Bannister, A.J. *et al.* Selective recognition of methylated lysine 9 on histone H3 by the HP1 chromo domain. *Nature* **410**, 120–124 (2001).
5. Lachner, M., O'Carroll, D., Rea, S., Mechtler, K. & Jenuwein, T. Methylation of histone H3 lysine 9 creates a binding site for HP1 proteins. *Nature* **410**, 116–120 (2001).
6. Strahl, B.D. & Allis, C.D. The language of covalent histone modifications. *Nature* **403**, 41–45 (2000).
7. Jenuwein, T. & Allis, C.D. Translating the histone code. *Science* **293**, 1074–1080 (2001).
8. Peng, H., Ivanov, A.V., Oh, H.J., Lau, Y.F. & Rauscher, F.J. 3rd. Epigenetic gene silencing by the SRY protein is mediated by a KRAB-O protein which recruits the KAP1 co-repressor machinery. *J. Biol. Chem.* **284**, 35670–35680 (2009).
9. Quivy, J.P. *et al.* A CAF-1 dependent pool of HP1 during heterochromatin duplication. *EMBO J.* **23**, 3516–3526 (2004).
10. Lomberk, G., Bensi, D., Fernandez-Zapico, M.E. & Urrutia, R. Evidence for the existence of an HP1-mediated subcode within the histone code. *Nat. Cell Biol.* **8**, 407–415 (2006).
11. Maison, C. *et al.* Higher-order structure in pericentric heterochromatin involves a distinct pattern of histone modification and an RNA component. *Nat. Genet.* **30**, 329–334 (2002).
12. Muchardt, C. *et al.* Coordinated methyl and RNA binding is required for heterochromatin localization of mammalian HP1alpha. *EMBO Rep.* **3**, 975–981 (2002).
13. Rudert, F., Bronner, S., Garnier, J.M. & Dolle, P. Transcripts from opposite strands of gamma satellite DNA are differentially expressed during mouse development. *Mamm. Genome* **6**, 76–83 (1995).
14. Lu, J. & Gilbert, D.M. Proliferation-dependent and cell cycle regulated transcription of mouse pericentric heterochromatin. *J. Cell Biol.* **179**, 411–421 (2007).
15. Kalitsis, P. & Choo, K.H.A. Centromere DNA of higher eukaryotes. in *The Centromere* (ed. Choo, K.H.A.) 97–140 (Oxford University Press, New York, 1997).
16. Heard, E. & Bickmore, W. The ins and outs of gene regulation and chromosome territory organisation. *Curr. Opin. Cell Biol.* **19**, 311–316 (2007).
17. Deng, Z., Norseen, J., Wiedmer, A., Riethman, H. & Lieberman, P.M. TERRA RNA binding to TRF2 facilitates heterochromatin formation and ORC recruitment at telomeres. *Mol. Cell* **35**, 403–413 (2009).
18. Wang, Q., Zhang, Z., Blackwell, K. & Carmichael, G.G. Vigilins bind to promiscuously A-to-I-edited RNAs and are involved in the formation of heterochromatin. *Curr. Biol.* **15**, 384–391 (2005).
19. Kuroda, M.I., Kernan, M.J., Kreber, R., Ganetzky, B. & Baker, B.S. The maleless protein associates with the X chromosome to regulate dosage compensation in *Drosophila*. *Cell* **66**, 935–947 (1991).
20. Irvine, K., Stirling, R., Hume, D. & Kennedy, D. Rasputin, more promiscuous than ever: a review of G3BP. *Int. J. Dev. Biol.* **48**, 1065–1077 (2004).
21. Shin, J.A. *et al.* SUMO modification is involved in the maintenance of heterochromatin stability in fission yeast. *Mol. Cell* **19**, 817–828 (2005).
22. Aagaard, L. *et al.* Functional mammalian homologues of the *Drosophila* PEV-modifier Su(Var)3–9 encode centromere-associated proteins which complex with the heterochromatin component M31. *EMBO J.* **18**, 1923–1938 (1999).
23. Hay, R.T. SUMO: a history of modification. *Mol. Cell* **18**, 1–12 (2005).
24. Meulmeester, E. & Melchior, F. Cell biology: SUMO. *Nature* **452**, 709–711 (2008).
25. Park-Sarge, O.K. & Sarge, K.D. Detection of SUMOylated proteins. *Methods Mol. Biol.* **464**, 255–265 (2009).
26. Jakobs, A. *et al.* Ubc9 fusion-directed SUMOylation (UFDS): a method to analyze function of protein SUMOylation. *Nat. Methods* **4**, 245–250 (2007).
27. Peters, A.H. *et al.* Loss of the Suv39h histone methyltransferases impairs mammalian heterochromatin and genome stability. *Cell* **107**, 323–337 (2001).
28. Loyola, A., Bonaldi, T., Roche, D., Imhof, A. & Almouzni, G. PTMs on H3 variants before chromatin assembly potentiate their final epigenetic state. *Mol. Cell* **24**, 309–316 (2006).

29. Smothers, J.F. & Henikoff, S. The hinge and chromoshadow domain impart distinct targeting of HP1-like proteins. *Mol. Cell. Biol.* **21**, 2555–2569 (2001).
30. Kerscher, O. SUMO junction-what's your function? New insights through SUMO-interacting motifs. *EMBO Rep.* **8**, 550–555 (2007).
31. Ouyang, J., Shi, Y., Valin, A., Xuan, Y. & Gill, G. Direct binding of CoREST1 to SUMO-2/3 contributes to gene-specific repression by the LSD1/CoREST1/HDAC complex. *Mol. Cell* **34**, 145–154 (2009).
32. Allshire, R.C. & Karpen, G.H. Epigenetic regulation of centromeric chromatin: old dogs, new tricks? *Nat. Rev. Genet.* **9**, 923–937 (2008).
33. Moazed, D. Small RNAs in transcriptional gene silencing and genome defence. *Nature* **457**, 413–420 (2009).
34. Blankenship, J.T. & Wieschaus, E. Two new roles for the *Drosophila* AP patterning system in early morphogenesis. *Development* **128**, 5129–5138 (2001).
35. Kanellopoulou, C. *et al.* Dicer-deficient mouse embryonic stem cells are defective in differentiation and centromeric silencing. *Genes Dev.* **19**, 489–501 (2005).
36. Murchison, E.P., Partridge, J.F., Tam, O.H., Cheloufi, S. & Hannon, G.J. Characterization of Dicer-deficient murine embryonic stem cells. *Proc. Natl. Acad. Sci. USA* **102**, 12135–12140 (2005).
37. Tsai, M.C. *et al.* Long noncoding RNA as modular scaffold of histone modification complexes. *Science* **329**, 689–693 (2010).
38. Savarese, F., Flahndorfer, K., Jaenisch, R., Busslinger, M. & Wutz, A. Hematopoietic precursor cells transiently reestablish permissiveness for X inactivation. *Mol. Cell. Biol.* **26**, 7167–7177 (2006).
39. Agrelo, R. *et al.* SATB1 defines the developmental context for gene silencing by Xist in lymphoma and embryonic cells. *Dev. Cell* **16**, 507–516 (2009).
40. Santos, F., Peters, A.H., Otte, A.P., Reik, W. & Dean, W. Dynamic chromatin modifications characterise the first cell cycle in mouse embryos. *Dev. Biol.* **280**, 225–236 (2005).
41. Puschendorf, M. *et al.* PRC1 and Suv39h specify parental asymmetry at constitutive heterochromatin in early mouse embryos. *Nat. Genet.* **40**, 411–420 (2008).
42. Probst, A.V. *et al.* A strand-specific burst in transcription of pericentric satellites is required for chromocenter formation and early mouse development. *Dev. Cell* **19**, 625–638 (2010).
43. Haaf, T. & Ward, D.C. Higher order nuclear structure in mammalian sperm revealed by *in situ* hybridization and extended chromatin fibers. *Exp. Cell Res.* **219**, 604–611 (1995).
44. Mayer, R. *et al.* Common themes and cell type specific variations of higher order chromatin arrangements in the mouse. *BMC Cell Biol.* **6**, 44 (2005).
45. Terranova, R., Sauer, S., Merkenschlager, M. & Fisher, A.G. The reorganisation of constitutive heterochromatin in differentiating muscle requires HDAC activity. *Exp. Cell Res.* **310**, 344–356 (2005).
46. Hajkova, P. *et al.* Chromatin dynamics during epigenetic reprogramming in the mouse germ line. *Nature* **452**, 877–881 (2008).
47. Solovei, I. *et al.* Nuclear architecture of rod photoreceptor cells adapts to vision in mammalian evolution. *Cell* **137**, 356–368 (2009).
48. Narita, M. *et al.* Rb-mediated heterochromatin formation and silencing of E2F target genes during cellular senescence. *Cell* **113**, 703–716 (2003).

ONLINE METHODS

Mouse cell lines. We cultured wild-type and *Suv39h* double-null MEFs (provided by T. Jenuwein)[27] and NIH 3T3 cells (ATCC #CRL-1658) as described[2]. We transfected MEFs and NIH 3T3 cells with Nucleofector Kit 2 (Amaxa) and Lipofectamine 2000 (Invitrogen), respectively, according to manufacturer's instructions.

Plasmids. We obtained plasmids encoding GFP-SUMO-1 from R. Hay, Myc-SUV39H1 from T. Jenuwein[22] and GST-HP1α full-length protein and fragments thereof (CD, CD+H, H and CSD) from R. Losson[49]. We carried out cloning using standard PCR-based techniques. We made e-HP1α, e-Ubc9 and e-SUMO-1Δ6 constructs by inserting HP1α (gift of R. Losson), Ubc9 (gift of J. Seeler) and SUMO-1Δ6 (from pEGFP-SUMO-1) fused to a HA-tag in the C terminus into a pcDNA5 vector (Invitrogen). We generated e-HP1α-Ubc9 and e-HP1α-SUMO-1 constructs by inserting the HP1α complementary DNA (cDNA) at the N terminus of the e-Ubc9 and the e-SUMO-1Δ6 plasmids, respectively. To avoid conjugation of e-HP1α-SUMO-1 into other proteins, we removed the last six C-terminal amino acids of SUMO-1, which contain the diglycine motif required for isopeptide bond formation. We generated HP1α and e-HP1α-Ubc9C93S point mutants using the QuickChange Site-Directed Mutagenesis Kit (Stratagene). To generate e-HP1αΔH and e-HP1αΔ-Ubc9 mutants, we made truncation contructs of e-HP1α and e-HP1α-Ubc9 in which the amino acids Met67 to Arg117 forming the hinge domain were deleted and replaced by a linker of two amino acids (isoleucine and aspartate). These truncation contructs led to the fusion of the chromo domain to the chromoshadow domain. We generated a GST-HP1α-hinge-chromoshadow domain and GST-HP1α-Ubc9 by subcloning from full-length GST-HP1α and e-HP1α-Ubc9, respectively. Each mutation and truncation was verified by sequencing.

Antibodies. We used: mouse monoclonal anti-HP1α (2HP-1H5-AS for immunofluorescence and 2HP-2G9-AS for protein blot; 1:1,000), anti-HP1β (1MOD-1A9-AS; 1:1,000) and anti-HP1γ (2MOD-1G6-AS; 1:1,000), all from Euromedex; rabbit polyclonal anti-vigilin (from D. Shapiro[50]; 1:3,000), rabbit polyclonal anti-RHA (PA-001, Vaxron; 1:10,000), mouse monoclonal anti-SUMO-1 (#33-2400; 1:500) and rabbit polyclonal anti–SUMO-2/3 (#51-9100; 1:250), both from Zymed; rat monoclonal anti-HA (#1867423, Roche; 1:2,000 for protein blot and 1:250 for immunofluorescence); mouse monoclonal anti-G3bp (#611126, BD Biosciences; 1:1,000); mouse monoclonal anti-Myc (ab32, Abcam; 1:500); rabbit polyclonal anti-GST (ab9085 Abcam; 1:1,000); rabbit polyclonal anti-GFP (sc-8334, Santa-Cruz; 1:500); rabbit polyclonal anti-H3K9me3 (#07-442, Upstate; 1:500); and mouse monoclonal anti-β actin (#A5441 Sigma; 1:20,000). For chromatin immunoprecipitations, we used a rabbit polyclonal HP1α antibody generated against the full-length GST-HP1α protein (Agro-Bio).

Nuclear extracts. After incubation in hypotonic Buffer A (20 mM HEPES-KOH pH 7.8, 5 mM potassium acetate, 0.5 mM $MgCl_2$ and 0.5 mM DTT) for 10 min at 4 °C, we disrupted NIH 3T3 cells by 25 strokes with a dounce homogenizer and separated the nuclei from the soluble proteins by centrifugation at 1,600*g*. After incubation of nuclear pellets in Buffer A containing 615 mM NaCl for 1.5 h at 4 °C followed by centrifugation at 14,000*g* for 20 min, we collected supernatant as the nuclear extract that we aliquoted and flash froze in liquid nitrogen. All buffers contained protease and phosphatase inhibitors (10 μg/ml pepstatin, 10 μg/ml leupeptin, 100 μM phenylmethanesulfonylfluoride (PMSF), 5 mM sodium fluoride and 10 mM β-glycerophosphate, plus or minus 20 mM N-ethylmaleimide (NEM; Sigma) when indicated.

Centromeric RNA pull down. The Maj9-2 and Min5-1 pCR4 plasmids contain 542 bp of the mouse major satellite DNA and 162 bp of minor satellite DNA, respectively (provided by T. Jenuwein)[51]. We subcloned a cDNA encoding a 234-bp repeat unit of the mouse major satellite DNA from pUC19-Sat15 (provided by A. Bird) into the pBS vector (Stratagene). We obtained biotinylated major (Maj1 from Sat15-pBS and Maj2 from Maj9-2 pCR4) and minor (Min from Min5-1 pCR4) RNAs by *in vitro* transcription with T7 or T3 RNA polymerases (Promega) in the presence of biotin RNA-labeling mix (Roche) at 37 °C for 2 h. After DNA digestion by RNase-free DNase I (Promega), we removed unincorporated rNTPs by a Sephadex G-50 quick spin column (Roche). For RNA pull down, we incubated 2 μg of biotinylated RNA with nuclear extracts in binding buffer (20 mM HEPES pH 7.6, 100 mM KCl, 2 mM EDTA, 0.01% Nonidet P-40 and 1% gelatin) with 200 μg/ml transfer RNA (tRNA), 4 mg/ml heparin and 80 U RNasin, plus or minus 20 mM NEM as indicated, for 30 min at room temperature (23 °C). For each binding reaction, we used 100 μl of streptavidin-coated magnetic beads (Dynabeads; Invitrogen) for 1 h at room temperature on a rotating wheel. After four washes with binding buffer containing 20 μg/ml tRNA and 0.1% Tween-20, followed by one more wash with 20 mM HEPES pH 7.6 plus 50 mM KCl, we eluted bound proteins with SDS-PAGE loading buffer and ran samples on NuPAGE 4–12% Bis-Tris gels (Invitrogen) with MOPS running buffer (Invitrogen). We stained gels with Coomassie brilliant blue.

Immunoprecipitations and protein blotting. We lysed NIH 3T3 cells 48 h post transfection, with lysis buffer (50 mM Tris-HCl pH 7.5, 150 mM NaCl, 5 mM EDTA, 15 mM $MgCl_2$, 1% Nonidet P-40 and 0.75% sodium deoxycholate), supplemented with protease and phosphatase inhibitors, and 20 mM NEM (Sigma). We incubated cell lysates corresponding to 4×10^6 cells with 40 μl of monoclonal anti-HA agarose-conjugated beads (Roche) for 2 h at 4 °C. After washing the beads with lysis buffer, we eluted the immunocomplexes with SDS-PAGE loading buffer and resolved the proteins by 4–12% Bis-Tris NuPAGE gels (Invitrogen) and transferred them to nitrocellulose membranes (Protran). For visualization of proteins after protein blots with the indicated antibodies, we used the Super Signal detection kit (Pierce).

Northwestern blotting. We resolved recombinant full-length GST-HP1γ and full-length GST-HP1α and fragments thereof by SDS-PAGE and transferred them to nitrocellulose. We incubated the membranes with *in vitro*–transcribed radioactively labeled RNAs in buffer containing 20 mM HEPES pH 7.6, 100 mM KCl, 2 mM EDTA and 0.01% Nonidet P-40 overnight at 23 °C. After three washes with the same buffer, we visualized bound radioactively labeled RNAs by autoradiography.

Immunofluorescence microscopy. We processed cells for immunostaining as described[11]. We used an epifluorescence photo microscope (DM6000B, Leica) piloted with MetaMorph software, a ×63 (NA 1.32) objective lens and an HQ2 CoolSNAP camera (Photometrics) for image acquisition. For all time course studies, we performed three independent experiments. For spot formation analysis, after image acquisition, we drew a scan line across the nucleus and measured the relative intensity of fluorescence across this line for signals corresponding to e-HP1α and Myc-SUV39H1 (ImageJ software). For immuno-RNA FISH, we acquired 50 optical sections separated by 0.2 μm with an Imager Z1 microscope (Zeiss) piloted with MetaMorph software and made Z projections. We quantified the localization of forward major transcripts at the periphery of the pericentric heterochromatin domains from a 3-dimensional (3D) image series (z-step 0.2 μm) of major RNA FISH/DAPI staining acquired on a DeltaVision system (Applied Precision, ×100 objective). For each nucleus, we manually scored the total number of RNA foci (f_{tot}) and the number of RNA foci at the periphery of DAPI-dense pericentric domains (f_{per}) using ImageJ software and the Image 5D plugin to allow co-visualization in 3D of the RNA FISH and DAPI signals. We determined the volume of the nuclei (V_{nuc}) and the volume of the individual pericentric domains (V_{dom}, DAPI dense) using the ImageJ software and the 3D Object Counter plugin. We calculated the volume of peripheral pericentric domain (V_{per}) as the difference between the volume corresponding to the pericentric domain with an increase of 20% of the radius of the domain ($V_{dom20\%}$, assuming a spherical form) and the volume of the domain ($V_{per} = V_{dom20\%} - V_{dom}$). We obtained the concentration of RNA foci (foci per μm^3) at the periphery from the ratio f_{per}/V_{per} and in the nucleus from the ratio $f_{tot}/(V_{nuc} - V_{dom})$. We removed the volume of the pericentric domains from total volume, given that RNA foci are never found within domains.

RNA and DNA FISH. For RNA FISH, after extraction with 0.5% Triton X-100 in CSK buffer (10 mM Pipes pH7, 100 mM NaCl, 300 mM sucrose, 3 mM $MgCl_2$, supplemented with 10 mM Vanadyl ribonucleoside complex (VRC)) for 5 min on ice, we fixed cells in 3% paraformaldehyde in PBS for 12 min and stored them in 70% EtOH at −20 °C overnight. Following dehydration in 80%,

doi:10.1038/ng.765

95% and 100% EtOH, we carried out hybridization with 0.4 μM locked nucleic acid (LNA) fluorescent probes (Exiqon) in 50% formamide (Sigma), ×2 SSC (Sigma), 10% dextran sulfate (Fluka), 10 mM VRC (NEB) and 2 mg/mL BSA (NEB) in a humid chamber for 35 min at 37 °C. After three washes in ×0.1 SSC for 5 min at 60 °C, we stained the DNA with DAPI staining and mounted the cells in VECTASHIELD (Vector Laboratories). For immuno-RNA FISH, we performed RNA FISH as described above. After post-hybridization washes, we post-fixed cells in 3% paraformaldehyde in PBS for 12 min and processed them for immunostaining. DNA FISH and immuno-DNA FISH were performed as described[2], except that here the hybridization mix contained LNA fluorescent probes (0.1 μM), and we performed post-hybridization washes in ×0.1 SSC (three times for 5 min) at 60 °C. The sequences of the LNA fluorescent probes are listed in **Supplementary Table 2**.

RT-PCR analysis. We performed RT-PCR analysis on HP1α-associated RNAs and on total RNA extracted from 3T3 cells with TRIzol (Invitrogen). We digested genomic DNA by incubation with DNase 1 (Sigma). We synthesized first-strand cDNA from 1 μg RNA in 20 μl buffer containing 1 μM forward (For)- or reverse (Rev)-specific primers for major or minor satellites, 0.5 mM dNTPs, 40 U/μl RNasin and 10 U/μl of SuperScript II reverse transcriptase (QIAGEN). We then amplified the generated cDNA by PCR using 1/2,000 and 1/250 dilutions of major and minor cDNA, respectively, and a PCR Master Kit (Roche) supplemented with 0.5 μM specific primers during 45 cycles. Primer sequences are listed in **Supplementary Table 2**.

Chromatin immunoprecipitation (ChIP). We extracted NIH 3T3 cells with Triton X-100 to remove soluble proteins as previously described[52] and cross-linked them with 1.5% formaldehyde in PBS for 20 min at room temperature. We then added 125 mM glycine for 20 min to quench any residual formaldehyde. After one wash with PBS, we collected the cells by scraping and resuspended them in ChIP buffer (20 mM Tris-HCl at pH 7.5, 200 mM NaCl, 0.2% Nonidet P-40, 1% gelatin and 80 U RNasin). We then sonicated the cells seven times for 30 s on high intensity (Bioruptor sonicator, CosmoBio Inc.) and centrifuged them at 10,000*g* for 5 min. We incubated approximately 200–300 μg of supernatant containing the soluble chromatin with 20 μl of sera against HP1α raised in the laboratory for 3 h at 4 °C. We used pre-immune sera as the negative control. Then we added 100 μl of Protein-A sepharose slurry (50% wt/vol, Amersham Biosciences) and incubated for 3 h at 4 °C on a rotating wheel. We recovered the immunoprecipitated chromatin by centrifugation, washed it five times with 1 ml of ChIP buffer and resuspended it in 10 mM Tris-HCl at pH 7.5, 1 mM EDTA and 0.2% SDS. We reversed the cross-link by incubation at 65 °C overnight. We then extracted the HP1α-associated RNAs with TRIzol (Invitrogen), and we performed RT-PCR analysis.

***In vitro* SUMOylation assays.** We produced recombinant proteins in *Escherichia coli* by expressing constructs corresponding to the GST-HP1α full-length protein and fragments thereof and GST-HP1α-Ubc9. We used the recombinant proteins in *in vitro* SUMOylation reactions using the SUMOlink kits (Active Motif) according to the manufacturer's instructions. We validated SUMOylation of HP1α and HP1α-Ubc9 by protein blot with GST antibodies. For analysis of the SUMOylated GST-HP1α hinge fragment by mass spectrometry, we used a total of 5 μg of GST-HP1α hinge and 10 μg of SUMO-1 protein. We ran 90% of the reaction mixture on a 4–12% Bis-Tris NuPAGE gel (Invitrogen) and stained the gel overnight with LabSafe GEL Blue stain (Biosciences) for later mass spectrometry analysis. We used the remaining 10% of the SUMOylation mixture for protein blotting with rabbit GST and rabbit SUMO-1 (Active Motif; 1:4,000 dilution) antibodies.

Mass spectrometry. We reduced, alkylated and trypsin digested slices (1 mm wide) cut from Coomassie blue–stained gels as previously described[53]. We dried extracted peptides and resolubilized them in solvent A (95/5 water/acetonitrile and 0.1% formic acid) before liquid chromatography tandem mass spectrometry (LC-MS/MS) analysis. We concentrated and separated them on an LC Packings system (Dionex S.A.) coupled to the nano-electrospray II ionization interface of a QSTAR Pulsar i (Applied Biosystems/MDS Sciex). HPLC mobile phases contained solvent A and solvent B (20/80 water/acetonitrile and 0.085% formic acid). We eluted bound peptides with a gradient of 5–50% of solvent B. We used information-dependent acquisition (IDA) to acquire MS/MS data, with experiments designed such that the two most abundant peptides were subject to collision-induced dissociation. We twice analyzed the data from the IDA experiments by using MASCOT software (Matrix Science) on an internal server, first without taxonomic restriction to reveal the presence of proteins of interest and mammalian contaminants, then again with the NCBI "*Mus musculus*" (mouse) database (National Library of Medicine, Bethesda, Maryland, USA, 2005 May 02; 2,452,561 total proteins entries and 41,362 *M. musculus* proteins entries). We converted the RAW files to the Mascot Generic Format (MGF) and submitted them to the Mascot search engine (version 1.0). We used the following parameters in the database search: full trypsin enzyme specificity; missed cleavages allowed = 1; peptide mass tolerance = 0.8 Da; fragment ion tolerance = 1 Da; monoisotopic molecular weight for both peptide and fragment ion masses; b/y ion search; and fixed carbamidomethyl cysteine modification. We manually validated all data using myProMS[54].

For SUMO-1 LC-MS/MS experiments, we used two different mass spectrometry platforms in parallel. We achieved peptide concentration and separation using an actively split capillary HPLC system (Ultimate 3000, Dionex) connected to each mass spectrometry platform. The first platform was a quadrupole time-of-flight (Q-TOF) mass spectrometer (QSTAR Elite, Applied Biosystems/MDS Sciex). We acquired a TOF-MS survey scan for 1 s over a mass range of 800–1,200 mass-to-charge ratio (m/z). We used an IDA method to acquire product ion scans on the three most intense 3+ ions per cycle over a mass range of 65–2,000 m/z excluding previously gated ions for 60 s. We used a Smart setting of 2.0. The second platform was an LTQ-Orbitrap XL mass spectrometer (Thermo Fisher Scientific) equipped with a nanospray source using a Pico-Tip (10 μm internal diameter (i.d.), New Objectives). We set the spray voltage to 2.2 kV and the temperature of the heated capillary to 200 °C. The mass spectrometer was operated in data-dependent mode to automatically acquire mass spectrometry and MS/MS spectra. We acquired full scan survey spectra (m/z 615–1,200) in the Orbitrap with a resolution of 100,000 at m/z 400 after accumulation of 1,000,000 charges. We sequentially isolated the five most intense ions and fragmented them in the linear ion trap by collision-induced dissociation after accumulation of 30,000 ions (normalized collision energy of 35%). Maximum inject times were 500 ms for full scans and 200 ms for MS/MS scans. Dynamic exclusion was enabled with an exclusion duration of 120 s. We calculated and used the monoisotopic m/z values for SUMO-1-GST-HP1α hinge-branched precursor peptides as described[55] to search for the corresponding ions (assignment was confirmed by manually interpreting all MS/MS spectra). We manually validated all reported MS/MS spectra. We considered only branched peptides having an extensive coverage of b and/or y ions. It was assumed that modified (SUMOylated) lysines cannot be cleaved by trypsin, and one trypsin missed cleavage was allowed.

49. Nielsen, A.L. *et al.* Heterochromatin formation in mammalian cells: interaction between histones and HP1 proteins. *Mol. Cell* **7**, 729–739 (2001).
50. Dodson, R.E. & Shapiro, D.J. Vigilin, a ubiquitous protein with 14 K homology domains, is the estrogen-inducible vitellogenin mRNA 3′-untranslated region-binding protein. *J. Biol. Chem.* **272**, 12249–12252 (1997).
51. Lehnertz, B. *et al.* Suv39h-mediated histone H3 lysine 9 methylation directs DNA methylation to major satellite repeats at pericentric heterochromatin. *Curr. Biol.* **13**, 1192–1200 (2003).
52. Martini, E., Roche, D.M., Marheineke, K., Verreault, A. & Almouzni, G. Recruitment of phosphorylated chromatin assembly factor 1 to chromatin after UV irradiation of human cells. *J. Cell Biol.* **143**, 563–575 (1998).
53. Fevrier, B. *et al.* Cells release prions in association with exosomes. *Proc. Natl. Acad. Sci. USA* **101**, 9683–9688 (2004).
54. Poullet, P., Carpentier, S. & Barillot, E. myProMS, a web server for management and validation of mass spectrometry-based proteomic data. *Proteomics* **7**, 2553–2556 (2007).
55. Matic, I. *et al. In vivo* identification of human small ubiquitin-like modifier polymerization sites by high accuracy mass spectrometry and an *in vitro* to *in vivo* strategy. *Mol. Cell. Proteomics* **7**, 132–144 (2008).